

# Spatial and Temporal Variations in Interstellar Absorption toward HD 72127AB\*

Daniel E. Welty<sup>1†</sup>, Thuso Simon<sup>2</sup>, and L. M. Hobbs<sup>3</sup>

<sup>1</sup>University of Chicago, Astronomy and Astrophysics Center, 5640 S. Ellis Ave., Chicago, IL 60637, USA; welty@oddjob.uchicago.edu

<sup>2</sup>University of New Mexico, Department of Physics and Astronomy, Albuquerque, NM 87131, USA; thuso@unm.edu

<sup>3</sup>University of Chicago, Yerkes Observatory, Williams Bay, WI 53191, USA; hobbs@yerkes.uchicago.edu

25 October 2018

## ABSTRACT

New optical spectra of Ca II and Na I toward HD 72127AB provide additional evidence for both spatial and temporal variations in the complex interstellar absorption along the two sight lines; archival UV spectra yield information on the abundances, depletions, and physical conditions in the gas toward HD 72127A. Similarities in the strengths of various tracers of interstellar material in the two lines of sight suggest that the total hydrogen column densities ( $N \sim 2.5 \times 10^{20} \text{ cm}^{-2}$ ) and the depletions and ionization in the main components at low LSR velocities also are similar. Toward HD 72127A, the main components are relatively cool ( $T \lesssim 900 \text{ K}$ ), but with depletions resembling those found in warm, diffuse disc clouds; the generally weaker components at higher velocities have much milder depletions, more like those found in halo clouds. Several trace neutral species – Ca I, Cr I, and Fe I – are much stronger toward HD 72127B, however. The column density of Cr I, for example, is about 30 times the value determined toward  $\zeta$  Oph (the only previous detection of that species in the ISM). Dielectronic recombination in warmer gas ( $T \gtrsim 5000 \text{ K}$ ) may be largely responsible for the enhanced abundances of those trace neutral species toward HD 72127B. If the main components toward HD 72127AB are associated with material in the Vela SNR, the differences in abundances and physical conditions occur on scales of about 1100 AU.

**Key words:** galaxies: ISM – ISM: abundances – ISM: lines and bands – ISM: structure – stars: individual (HD 72127).

## 1 INTRODUCTION

Small-scale (sub-parsec) spatial structure in the Galactic interstellar medium (ISM) has been revealed via a variety of methods: multi-epoch H I observations of pulsars (Frail et al. 1994; Stanimirović et al. 2003), VLBI observations of extended extragalactic radio sources (Dieter, Welch, & Romney 1976; Brogan et al. 2005), optical spectra of interstellar absorption lines toward binary/multiple star systems and star clusters (Kemp, Bates, & Lyons 1993; Watson & Meyer 1996; Points, Lauroesch, & Meyer 2004), and monitoring of the optical/UV absorption-line profiles toward stars either with significant proper motions or located behind disturbed regions (Hobbs et al. 1991; Rollinde et al. 2003; Welty 2007).

Understanding the nature and origin(s) of that small-scale structure in predominantly neutral gas, however, has been difficult. Observations of variations in Na I absorption, for example, seemed to imply local hydrogen densities ( $n_{\text{H}}$ ) of thousands per  $\text{cm}^3$  – similar to the values inferred more directly from the small-scale variations in H I, but much higher than would be expected for clouds in thermal pressure equilibrium at typical values  $n_{\text{H}}T \sim 2500 \text{ cm}^{-3}\text{K}$  (Jenkins & Tripp 2001). In principle, the observed small-scale structures might be due to geometrical (Heiles 1997), statistical (Deshpande 2000), and/or physical (Lauroesch & Meyer 2003) properties of the interstellar clouds. Recent studies combining optical and UV absorption-line data have suggested that at least some of the variations reflect differences in physical conditions (e.g., density, ionization) rather than overall hydrogen column density (Lauroesch et al. 1998; Welty 2007) – but that would not explain the variations seen directly in  $N(\text{H I})$  in other cases. Summaries of recent observational and theoretical studies of small-scale interstellar structure may be found in Haverkorn & Goss (2007).

\* Based on observations collected at the European Southern Observatory, Chile, under program 72.C-0682, and on observations made with the NASA/ESA *Hubble Space Telescope*, which is operated by the Association of Universities for Research in Astronomy, Inc., under NASA contract NAS5-26555.

† Visiting observer, European Southern Observatory

Observations of stars behind the Vela supernova remnant (SNR) provided some of the first (and most striking) indications of small-scale spatial and temporal variability in interstellar absorption lines (Thackeray 1974; Hobbs, Wallerstein, & Hu 1982; Danks & Sembach 1995; Cha & Sembach 2000). Such variations – seen toward at least seven stars in that region – are not entirely unexpected, given the presence of gas at relatively high velocities within the SNR (Wallerstein, Silk, & Jenkins 1980; Danks & Sembach 1995; Cha & Sembach 2000). The spatial and temporal differences in the optical lines of Na I and Ca II toward the binary system HD 72127AB have been particularly notable (Thackeray 1974; Hobbs et al. 1982, 1991; Welty, Morton, & Hobbs 1996; Cha & Sembach 2000). That system, consisting of a B2 III primary [ $V = 5.20$ ;  $E(B - V) = 0.10$ ] and a B2.5 V secondary [ $V = 7.09$ ;  $E(B - V) = 0.10$ ] at  $(l, b) = (262.57, -3.36)$ , is located behind the edge of a filamentary structure seen in H $\alpha$  emission, less than a degree away from the Vela pulsar. At a distance of about 480 pc, however, HD 72127AB is well behind the SNR, which is at about 250 pc (Cha, Sembach, & Danks 1999). The 4.5 arcsec separation between the two stars corresponds to a transverse distance of about 2200 AU at the stellar distance and about 1100 AU at the distance to the SNR. Thackeray (1974) first noted differences in the very broad, very strong ( $\gtrsim 500$  mÅ) interstellar Ca II K lines toward the two stars; Hobbs et al. (1981) then reported both corresponding differences in the Na I D lines and temporal changes in the profile of the Ca II line toward HD 72127A. Detailed fits to a series of Ca II and Na I profiles obtained between 1981 and 1988 toward HD 72127A indicated continuing variations in the column densities and/or velocities of many of the components – particularly those at low LSR velocities (Hobbs et al. 1991); high Ca II/Na I ratios for the higher velocity components are suggestive of significant grain disruption. Moderate-resolution UV spectra of the two stars obtained with the *Hubble Space Telescope* Goddard High Resolution Spectrograph (*HST* GHRS) revealed both similarities and differences in the equivalent widths of the lines from several dominant ions; analysis of the C I fine-structure excitation implied that some of the gas in both sight lines was characterized by fairly high thermal pressures (Wallerstein et al. 1995a; Wallerstein, Vanture, & Jenkins 1995b).

In this paper, we discuss new optical spectra of both HD 72127A and HD 72127B, obtained in 2003 with the ESO VLT Ultraviolet and Visual Echelle Spectrograph (UVES), and previously unpublished UV spectra of HD 72127A, obtained in 1992 with the *HST* GHRS. The optical and UV spectra reveal continuing temporal changes in the interstellar absorption toward those two stars and provide new information on the abundances and physical conditions in the gas. In Section 2, we describe the observed spectra and our reduction and analysis techniques. In Section 3, we discuss the elemental abundances and depletions in the gas, the temporal changes in various features, the differences in absorption between the two sight lines, and the remarkably strong absorption from some trace neutral species seen toward HD 72127B. In Section 4, we provide a summary of our results.

## 2 DATA

### 2.1 Observations and data processing

Optical spectra of HD 72127A and HD 72127B were obtained on 2003 November 14 using the ESO/VLT UT2 telescope and UVES spectrograph (Dekker et al. 2000), during a run devoted primarily to observations of weak atomic and molecular interstellar lines in the Magellanic Clouds (Welty et al. 2006; Welty & Crowther, in preparation). The standard dichroic 1 390/564 setting and a slit width corresponding to 0.7 arcsec were used to obtain nearly complete coverage of the wavelength range 3260–6680 Å (on three CCD detectors: two EEV CCD-44 and one MIT/LL CCID-20) at resolutions of about 4.5 km s<sup>-1</sup> in the blue and about 4.9 km s<sup>-1</sup> in the red. This setup includes lines from Na I (U and D doublets at 3302 and 5889/5895 Å), Ca I (4226 Å), Ca II (3933/3968 Å), and Ti II (3383 Å); the strongest lines from CH (4300 Å), CH<sup>+</sup> (4232 Å), and CN (3874 Å); and a number of the diffuse interstellar bands. Standard routines within IRAF were used to remove bias and to divide sections of the 2-D images containing the spectral order(s) of interest by a normalized flat-field derived from quartz lamp exposures. The 1-D spectra then were extracted from the flat-fielded image segments via the APEXTRACT routines, using variance weighting (with the appropriate values for read noise and gain for each detector). Wavelength calibration was accomplished via Th-Ar lamp exposures, which were obtained at the beginning and end of each night, using the thorium rest wavelengths tabulated by Palmer & Engelman (1983). The spectra were then normalized via Legendre polynomial fits to the continuum regions surrounding the interstellar (and stellar) absorption lines. Equivalent widths for the various interstellar absorption features were measured from those normalized spectra. The empirical signal-to-noise (S/N) ratios measured in the continuum regions are typically  $\sim 100$ –200 per half resolution element – yielding  $3\sigma$  uncertainties or detection limits for weak, unresolved absorption lines of 1–2 mÅ. Equivalent widths measured for various interstellar lines toward several other Galactic stars observed during the run show very good agreement with previously reported values (Gredel et al. 1991, 1993; Albert et al. 1993; Welty et al. 1999b). Observations of the bright, nearby, rapidly rotating star  $\psi^2$  Aqr were used to check for weak atmospheric absorption features and instrumental artefacts near the interstellar lines of interest.

UV spectra of HD 72127A were obtained in 1992 April and November with the *HST* GHRS, under GO programs 2251 and 3993 (L. M. Hobbs, PI). The data set includes 13 high-resolution (FWHM = 3.3–3.7 km s<sup>-1</sup>) ECH-B settings, with central wavelengths from 1745 to 2800 Å, and ten medium-resolution (FWHM = 13–20 km s<sup>-1</sup>) G160M settings, with central wavelengths from 1135 to 1664 Å. Multiple, slightly offset sub-exposures were obtained at each setting – using the WSCAN procedure for the ECH-B spectra and the FP-SPLIT procedure for the G160M spectra – in order to identify and reduce the effects of detector fixed-pattern noise. The individual sub-exposures for each wavelength setting were aligned via fits to the interstellar absorption features, cleaned, and co-added; the summed spectra were then normalized via Legendre polynomial fits to the continuum regions. The empirical S/N ratios in the normalized spectra range from about 35 to 100 per half resolution

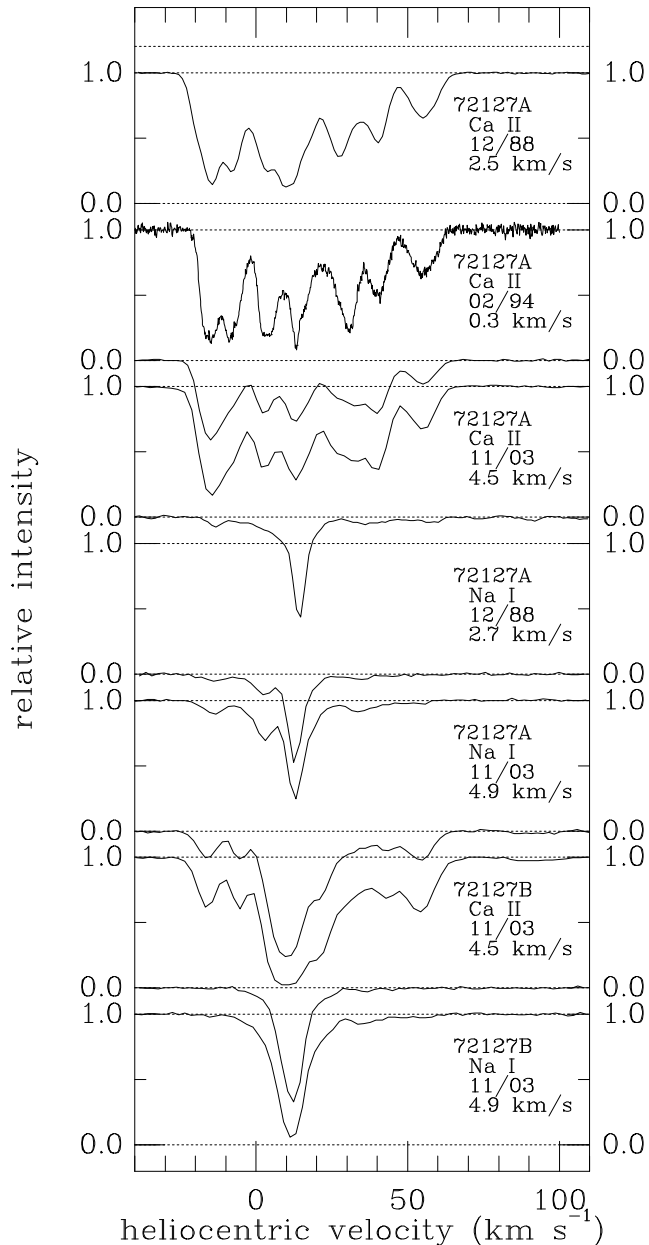


**Figure 1.** Interstellar Na I and Ca II profiles toward HD 72127A and HD 72127B. For each profile (or pair of profiles), the sight line, species, observation date, and resolution are given at the right. The UVES spectra (2003 Nov) reveal striking differences between the profiles for the two lines of sight, which are separated by only 4.5 arcsec. Several earlier profiles toward HD 72127A (Hobbs et al. 1991; Welty et al. 1996) are included to show temporal variations. Most of the components in Ca II exhibit some change over the 15-year span represented here.

element for the ECH-B data and from about 80 to 150 for the lower resolution G160M data. More detailed discussions of the GHRS data and our adopted reduction and analysis procedures may be found in Welty et al. (1999b).

## 2.2 Spectra and equivalent widths

The normalized line profiles for Ca II and Na I toward HD 72127A and HD 72127B are shown in Fig. 1. In each

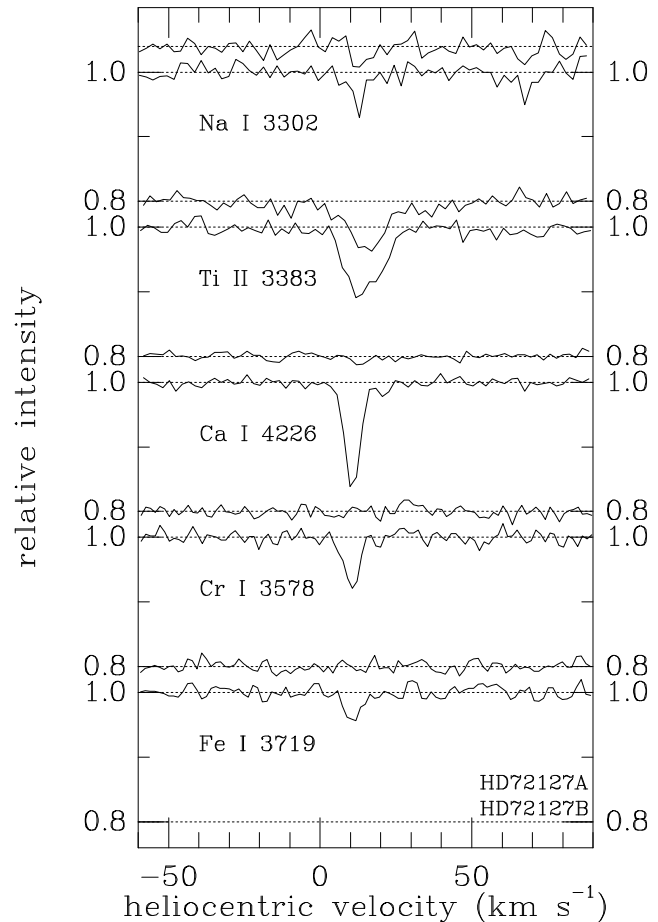


**Figure 2.** Profiles of weaker interstellar lines toward HD 72127A (upper for each pair) and HD 72127B (lower for each pair) observed with UVES. The weaker member of the Na I  $\lambda$ 3302 doublet is seen near  $+70 \text{ km s}^{-1}$ . The lines from Na I and Ti II are similar in strength toward the two stars, but the lines from Ca I, Cr I, and Fe I are much stronger toward HD 72127B.

case, the stronger member of the doublet (if present) is shown at a continuum level of 1.0, and the weaker member of the doublet (if present) is offset by  $+0.2$ . Velocities with respect to the local standard of rest (LSR) may be obtained by subtracting  $13.4 \text{ km s}^{-1}$  from the heliocentric velocities shown in the figure<sup>1</sup>. Several previously observed profiles for HD 72127A – Ca II and Na I from 1988 (FWHM  $\sim 2.5$ – $2.7 \text{ km s}^{-1}$ ; Hobbs et al. 1991) and Ca II from 1994 (FWHM  $\sim 0.3 \text{ km s}^{-1}$ ; Welty et al. 1996) – are included for comparison. Spectra of some of the weaker optical lines are shown in Fig. 2, where the profile for HD 72127A is offset above the one for HD 72127B in each case (and note the expanded vertical scale for all the lines). Profiles of some of the UV absorption lines toward HD 72127A are shown in Fig. 3, where (again) the vertical scale has been expanded for the weaker lines. Equivalent widths for the various lines measured from the normalized optical and UV spectra are listed in Table 1; for comparison, values reported for Mg II, S II, and Ge II by

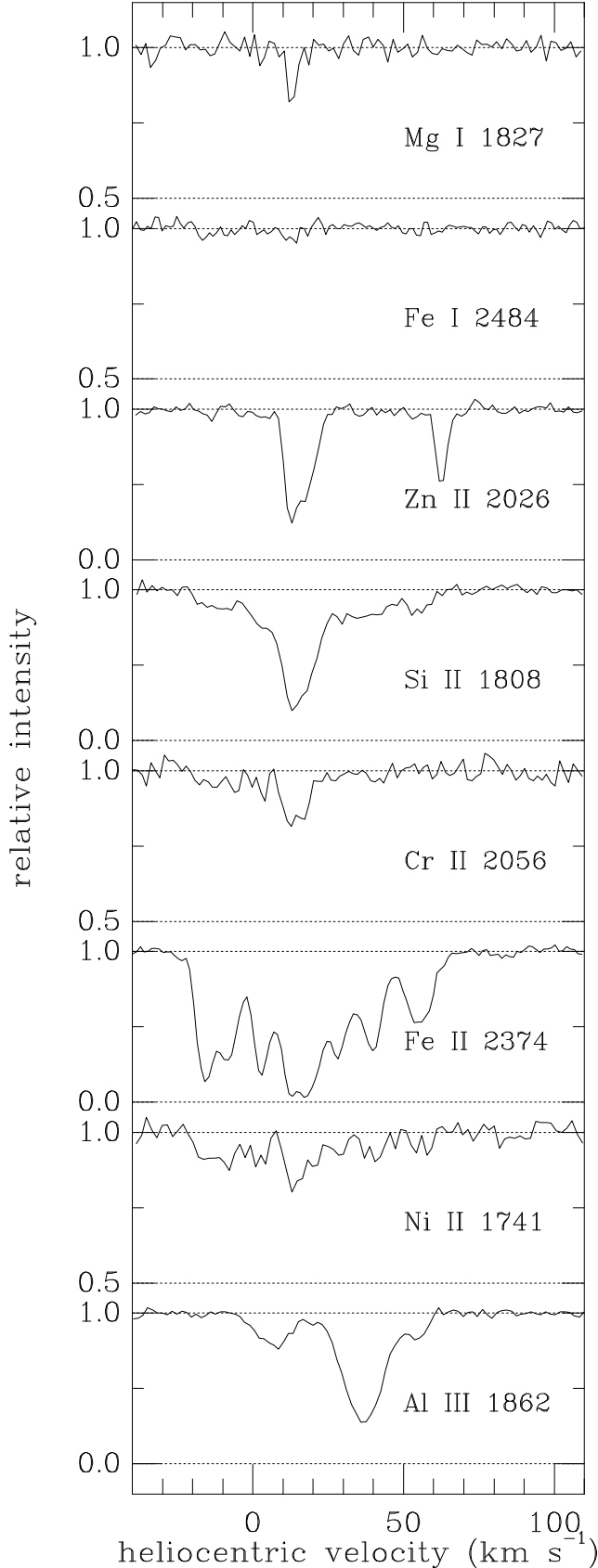


**Figure 3.** Selected UV absorption lines toward HD 72127A, obtained in 1992 with the *HST* GHRS, at resolutions of about 3.3–3.7 km s<sup>-1</sup>. The absorption near 60 km s<sup>-1</sup> in the Zn II spectrum is due to Mg I. Note the expanded vertical scale for several of the weaker lines.

**Table 1.** Equivalent widths.

Species	$\lambda$	$\log(f\lambda)$	HD 72127A	HD 72127B
O I	1355.5977	-2.803	<2.6	–
Na I	3302.3690	1.472	2.1±0.9	4.0±1.0
	3302.9780	1.170	1.9±0.8	2.7±1.0
	5889.9510	3.586	216.0±4.2	277.4±4.2
Mg I	5895.9242	3.285	135.9±4.0	187.6±3.3
	1827.9351	1.646	4.4±0.8	–
Mg II	2026.4768	2.360	18.3±1.3	–
	1239.9253	-0.106	14.8±1.7	–
–	–	–	[14.9]	[13.0]
–	1240.3947	-0.355	9.5±1.2	–
–	–	–	[8.6]	[8.0]
Al I	3944.0060	2.664	<1.1	<1.1
Al III	1854.7184	3.016	169.1±2.6	–
	1862.7910	2.714	100.6±2.2	–
Si I	2515.0725	2.725	1.8±0.4	–
Si II	1808.0129	0.575	115.1±4.1	–
S II	1250.5780	0.832	[111.5]	[104.0]
	1253.8050	1.136	[177.1]	[177.1]
	1259.5180	1.320	[209.0]	[204.3]
Cl I	1347.2396	2.314	6.2±2.2	–
Ca I	4226.7280	3.874	1.0±0.4	16.0±0.9
Ca II	3933.6614	3.392	531.8±1.9	508.4±2.4
	3968.4673	3.092	327.4±2.0	339.2±3.6
Ti I	3635.4620	2.962	<2.0	<1.6
Ti II	3383.7588	3.083	17.0±2.6	21.3±4.2
Cr I	3578.6840	3.117	<1.7	5.4±0.7
	3593.4810	3.019	–	5.5±0.6
	3605.3210	2.911	–	4.5±0.6
	4254.3320	2.670	–	2.7±0.4
	4274.7960	2.556	–	1.8±0.4
	4289.7160	2.427	–	1.2±0.4
	2056.2569	2.326	22.4±4.5	–
2062.2361	2.195	17.7±4.0	–	
Mn I	4030.7530	2.357	<1.2	<1.2
Fe I	2484.0209	3.131	1.7±0.5	–
	2523.6083	2.710	0.9±0.3	–
	3440.6057	1.910	–	1.3±0.6
	3719.9347	2.184	<1.3	3.5±0.7
	3859.9114	1.923	–	2.1±0.4
Fe II	2249.8768	0.612	35.0±3.1	–
	2374.4612	1.871	384.0±3.3	–
Ni I	3369.5656	1.913	<2.2	<2.6
Ni II	1741.5531	1.871	32.3±5.5	–
Zn II	2026.1370	3.007	56.3±3.6	–
	2062.6604	2.705	42.6±2.9	–
Ge II	1237.0589	3.183	2.9±1.1	–
–	–	–	[4.0]	[<2.6]

Entries are equivalent width  $\pm 1\sigma$  uncertainty (mÅ); limits are  $3\sigma$ . Wavelengths (in air above 3000 Å) and  $f$ -values are from Morton (2003). Values for lines above 3000 Å are from 2003 UVES spectra; values for lines below 3000 Å are from 1992 GHRS spectra; values in square brackets are from 1992–1993 GHRS spectra (Wallerstein et al. 1995).

Wallerstein et al. (1995b) (from GHRS spectra obtained in 1992 and 1993) are given in square brackets.

In both sight lines, the trace neutral species (e.g., Na I,

<sup>1</sup> The conversion to LSR velocities assumes a solar motion of 20 km s<sup>-1</sup> toward  $(\alpha, \delta) = (18^{\text{h}}, 30^{\circ})$ .

Mg I) are found primarily in an apparently single component at +10 to +13 km s<sup>-1</sup> ( $v_{\text{LSR}} \sim -3$  to 0 km s<sup>-1</sup>), with much weaker absorption extending from about -20 to +55 km s<sup>-1</sup>. Toward HD 72127A, the absorption from dominant ions of typically mildly depleted elements (e.g., Zn II) is concentrated in several components between about +10 and +20 km s<sup>-1</sup>, with hints of much weaker absorption at lower and higher velocities. The absorption from dominant ions of typically more severely depleted elements (e.g., Si II, Fe II) also is strongest between +10 and +20 km s<sup>-1</sup>, but becomes increasingly prominent at both lower and higher velocities for the species most affected by depletion. Ca II – which can be affected by both ionization and depletion (e.g., Welty et al. 1996) – shows moderately strong absorption over the entire velocity range.

### 2.3 Profile fits

Multicomponent fits to observed complex absorption-line profiles enable blended lines and components to be disentangled, account explicitly for saturation effects in the stronger components, and allow spectra obtained at (somewhat) different resolutions to be compared. The method of profile fitting was therefore used to estimate column densities ( $N$ ), line widths ( $b \sim \text{FWHM}/1.665$ ), and velocities ( $v$ ) for the individual components discernible in the spectra (e.g., Hobbs et al. 1991; Welty, Hobbs, & Morton 2003). For each species, the minimum number of components needed to achieve ‘satisfactory’ fits to the detected lines was adopted (given the resolution and S/N ratios characterizing the spectra and assuming that each component may be represented by a symmetric Voigt profile). Multiple lines for a given species (e.g., the two lines of Ca II) were fitted simultaneously. The structure determined for Ca II was used to estimate individual component column densities for Ti II from the weak  $\lambda 3383$  lines. The lines from Si II, Cr II, Fe II, Ni II, and Zn II seen in the GHRS ECH-B spectra were fitted simultaneously – using a common velocity structure but adjusting the component column densities (and some  $b$ -values) for each species.

The adopted interstellar component parameters derived from the UVES spectra of HD 72127A and HD 72127B are listed in Table 2; the component parameters obtained from the simultaneous fit to the GHRS ECH-B spectra of HD 72127A are given in Table 3. For each component in each sight line, Table 2 gives the component number, the heliocentric velocity and  $b$ -value (for Na I and Ca II), and the column densities of Na I, Ca I, Ca II, and Ti II. Component column densities or  $b$ -values in square brackets were fixed, but relatively well determined in the fits; values in parentheses also were fixed, but are less well determined. For Na I, the column density of the strongest component in each sight line was fixed at a value consistent with that derived from the weak  $\lambda 3302$  doublet; the parameters for the other components were derived from fits to the much stronger Na I D lines. Independent fits to the profiles of the Na I D lines and the Ca II H and K lines yielded rather similar component velocities (in both sight lines), and components seen in the two species are considered to be associated if the velocities agree within about 1–2 km s<sup>-1</sup>.

The 1  $\sigma$  uncertainties given for  $N$ ,  $b$ , and  $v$  in Tables 2 and 3 reflect only photon noise, and thus should be considered as lower limits to the true uncertainties. Consideration

**Table 4.** Column densities.

Species	HD 72127A	HD 72127B	23 Ori SLV	$\zeta$ Oph B
H <sub>tot</sub>	[20.40]	[20.40]	20.71	21.15
O I	<17.14	–	17.29	17.63
Na I	12.46±0.12	12.66±0.06	13.41	13.85
Mg I	12.92±0.04	–	13.80	13.80
Mg II	15.29±0.04	–	15.57	15.32
Si I	11.20±0.11	–	11.79	–
Si II	15.43±0.01	–	15.37	15.34
Al I	<10.83	<10.83	<11.53	<10.22
Cl I	12.52±0.16	–	13.29	14.48
Ca I	9.58±0.08	10.76±0.02	10.20	9.46
Ca II	12.99±0.01	13.22±0.02	12.04	11.71
Ti I	<10.88	<10.79	<10.72	–
Ti II	11.68±0.06	11.78±0.08	11.15	11.03
Cr I	<10.61	11.26±0.02	<10.59	9.78
Cr II	12.80±0.04	–	12.64	12.39
Mn I	<11.17	<11.17	10.23	<11.30
Mn II	–	–	13.08	13.20
Fe I	10.77±0.11	11.89±0.03	11.34	11.23
Fe II	14.69±0.01	–	14.30	14.32
Ni I	<11.95	<12.03	<10.26	<11.40
Ni II	13.48±0.03	–	12.90	12.91
Zn II	12.72±0.01	–	13.24	–
Ge II	11.25±0.17	–	11.86	11.75

Entries are  $\log [N \text{ (cm}^{-2}\text{)}] \pm 1\sigma$  uncertainty, based on fits to the line profiles; limits are  $3\sigma$ . Values for 23 Ori SLV (main) components are from Welty et al. (1999b), except for Na I, Ti I, and Cr I, which are from new UVES data. Values for  $\zeta$  Oph B (main) component are from Welty & Hobbs (2001), Welty et al. (2003), and references therein.

of the effects of uncertainties in continuum placement (most significant for the stronger lines) and of allowing fixed parameters (usually  $b$ ) to vary would increase the uncertainties in the various parameters (primarily  $N$ ). In view of the statistics of component width and separation obtained from higher resolution, higher S/N spectra of Galactic targets (Welty et al. 1994, 1996; Welty & Hobbs 2001), however, it is likely that the ‘true’ component structures are even more complex than those listed in the tables – and that uncertainty may well be even more significant for the individual component parameters. Differences in the component velocities derived for Na I and Ca II, for example, may be due to component-to-component differences in relative abundances in an underlying more complex structure. Higher resolution spectra of Ca II toward HD 72127A do exhibit more complex structure (Fig. 1; Welty et al. 1996). Differences between the component velocities derived from optical and UV spectra of HD 72127A may reflect (in addition) possible temporal variations between 1992 and 2003.

The total sight line column densities are given in Table 4, with values for the main neutral components toward 23 Ori (Welty et al. 1999b) and  $\zeta$  Oph (Welty et al. 2003 and references therein) given for comparison. In all cases, the values derived from the profile fits are consistent with estimates or limits based on integrating the ‘apparent’ optical depth over the absorption lines; the total sight line column densities are in most cases fairly well determined.

**Table 2.** Component structures (optical data).

Comp	Na I			Ca I		Ca II		Ti II	Ca II/Na I	Ca II/Ti II
	$v$ (km s <sup>-1</sup> )	$b$ (km s <sup>-1</sup> )	$N_{10}$ (cm <sup>-2</sup> )	$N_9$ (cm <sup>-2</sup> )	$v$ (km s <sup>-1</sup> )	$b$ (km s <sup>-1</sup> )	$N_{10}$ (cm <sup>-2</sup> )	$N_{10}$ (cm <sup>-2</sup> )		
HD 72127A										
1					-27.7±2.1	(3.0)	1.0±0.5			
2	-13.8±0.3	4.4±0.5	9.8±0.6		-15.4±0.1	3.2±0.1	218.3±3.8	2.6±1.4	22.3	~84.0
3					-8.2±0.1	(4.0)	112.6±3.0	2.0±1.5		~56.3
4	-1.1±0.6	(3.0)	8.4±1.2							
5	3.7±0.2	(2.0)	21.3±1.4		2.9±0.1	3.3±0.2	120.1±3.0	4.7±1.3	5.6	25.6
6	12.8±0.1	1.2±0.1	[250.0±70.]	3.8±0.7	12.6±0.2	3.6±0.4	148.4±12.	15.9±1.6	0.6	9.3
7	18.8±0.2	(3.0)	14.0±0.8		18.3±0.5	(3.0)	41.3±9.4	13.6±1.5	3.0	3.0
8					26.0±0.2	(3.0)	67.1±1.8	2.8±1.4		~24.0
9	32.8±0.5	(4.0)	7.4±0.7		32.3±0.2	(3.0)	81.6±2.2	3.3±1.4	11.0	~24.7
10	40.7±1.3	(4.0)	3.0±0.6		40.0±0.1	3.8±0.1	130.2±2.9	3.0±1.4	43.4	~43.4
11	52.0±1.3	(5.0)	2.5±0.5		54.7±0.1	4.9±0.1	61.6±1.0		24.6	
HD 72127B										
1	-15.1±1.3	(2.0)	1.0±0.4		-16.0±0.1	3.5±0.1	58.4±1.1		58.4	
2					-5.4±0.1	2.5±0.2	51.7±1.2	1.7±1.2		~30.4
3	-1.1±0.4	(2.5)	6.9±0.7							
4	6.5±0.4	(3.0)	31.7±4.3		4.3±0.3	(3.0)	113.1±17.		3.6	
5	12.2±0.1	2.5±0.1	[400.0±55.]	57.9±1.2	10.5±0.1	(4.0)	1060.0±65.	28.4±1.9	2.7	37.3
6	21.4±0.2	(3.5)	18.2±0.7	5.5±0.9	21.0±0.1	(4.0)	185.7±3.0	20.2±1.5	10.2	9.2
7					29.4±0.2	(3.0)	41.2±1.5			
8	34.7±0.4	(3.0)	5.7±0.5		35.7±0.3	(3.0)	27.2±1.3		4.8	
9	43.3±1.2	(4.0)	2.7±0.5		42.9±0.2	(3.0)	36.9±1.2		13.7	
10	54.2±1.2	(4.0)	2.1±0.5		53.8±0.1	5.6±0.1	90.4±1.6	3.5±1.5	43.0	25.8
11					88.0±1.0	(4.0)	4.0±0.8			
12					96.9±1.3	(4.0)	3.3±0.8			

The subscript on each column density header indicates the power of ten by which the listed value of that species should be multiplied. Toward HD 72127B, Cr I and Fe I are detected, with  $[N, v]$  equal to  $[(1.8±0.1)×10^{11}, 11.0±0.1]$  and  $[(7.8±0.6)×10^{11}, 10.6±0.2]$ , respectively.

**Table 3.** Component structures (HD 72127A UV data).

Comp	$v$ (km s <sup>-1</sup> )	$b$ (km s <sup>-1</sup> )	$N(\text{Zn II})$ (10 <sup>10</sup> cm <sup>-2</sup> )	$N(\text{Si II})$ (10 <sup>13</sup> cm <sup>-2</sup> )	$N(\text{Cr II})$ (10 <sup>11</sup> cm <sup>-2</sup> )	$N(\text{Fe II})$ (10 <sup>12</sup> cm <sup>-2</sup> )	$N(\text{Ni II})$ (10 <sup>12</sup> cm <sup>-2</sup> )	Fe II/Zn II
$N(3\sigma)$			9.0	3.5	4.5	2.5	2.0	
1	-24.3±1.2	(3.0)	–	–		1.1±0.3		–
2	-15.9±0.1	2.5	–	6.6±0.9	6.0±1.3	59.8±2.8	2.9±0.6	>665
3	-8.5±0.2	4.0	–	11.8±1.1	6.8±1.5	52.7±2.4	4.8±0.7	>585
4	2.9±0.1	2.8	17.3±3.8	24.6±1.3	5.8±1.3	54.6±1.4	3.4±0.6	315
5	13.2±0.2	[3.7]	338.2±13.	111.7±5.1	26.7±1.9	115.1±7.7	6.5±0.7	35
6	19.5±0.3	[4.0]	150.5±7.7	58.2±3.5	9.2±2.1	85.1±1.7	3.9±0.7	55
7	28.0±0.1	2.4	–	7.7±1.1	3.9±1.4	31.1±1.7	2.2±0.6	>345
8	32.9±0.5	(3.5)	–	13.7±1.3	–	15.1±1.7	–	>170
9	39.9±0.1	3.4	5.0±3.9	12.0±1.8	4.4±1.4	37.4±1.0	3.5±0.6	750
10	44.6±1.2	(3.5)	–	5.5±1.4	–	–	–	–
11	54.7±0.2	5.7	–	16.6±2.0	–	32.9±1.2	2.5±0.7	>365
12	57.8±0.8	(2.0)	–	–	–	2.3±1.0	–	–
10–20 km s <sup>-1</sup>			488.7±15.	169.9±6.2	35.9±2.8	200.2±7.9	10.4±1.0	40
outliers			<71.0	98.1±5.1	<36.6	286.8±7.7	19.5±1.7	>405
total			(526.0±18.)	268.0±8.0	(63.0±5.0)	487.0±11.	29.9±2.0	95

Total column densities for Zn II and Cr II in parentheses should be considered as lower limits, as not all components were detected.

### 3 DISCUSSION

#### 3.1 Abundances and depletions

In view of the spectral types of HD 72127A and HD 72127B, it is likely that the Lyman- $\alpha$  absorption observed toward the two stars (in archival *IUE* spectra) is an inseparable blend of stellar and interstellar components. Several indirect methods thus have been used to estimate the interstellar hydrogen column densities toward the two stars:

(1) The first makes use of the strong, nearly linear correlation observed between the equivalent width of the diffuse interstellar band (DIB) at 5780 Å and  $N(\text{H I})$  (e.g., Herbig 1993, 1995; Welty et al. 2006; D. G. York et al., in preparation). The equivalent widths estimated from our UVES spectra –  $W(5780) = 15 \pm 6$  mÅ for HD 72127A and  $W(5780) = 12 \pm 5$  mÅ for HD 72127B – suggest  $\log[N(\text{H I})]$  of about 20.2 for HD 72127A and about 20.1 for HD 72127B. The observed  $W(5780)$  are somewhat low, relative to the corresponding  $N(\text{Na I})$ , however, suggesting that the 5780 Å DIB may be weaker than usual toward HD 72127AB – as has been observed, for example, toward some Galactic and Magellanic Clouds targets (Herbig 1993; Welty et al. 2006). The  $N(\text{H I})$  estimated from  $W(5780)$  might thus be best viewed as lower limits.

(2) An estimate for  $N(\text{H})$  toward HD 72127A may be obtained from the observed column density of Zn II, as zinc is generally only very mildly depleted in diffuse interstellar clouds. If the depletion of zinc  $D(\text{Zn}) = -0.2$  dex (typical for warm diffuse gas), then  $\log[N(\text{Zn II})] = 12.72$  implies that  $\log[N(\text{H})]$  would be about 20.3, for a solar zinc abundance of  $-7.37$  dex (Lodders 2003). Fits to the lower resolution G160M spectra of the S II lines at 1250, 1253, and 1259 Å using the component structures found for Zn II and Si II yield consistent estimates for  $N(\text{H})$ , assuming a solar abundance of  $-4.81$  dex and no depletion for sulphur.

(3) If the typical Galactic gas-to-dust ratio  $\log[N(\text{H})/E(B - V)] = 21.71$  (e.g., Welty et al. 2006) applies to the sight line toward HD 72127AB, then the observed  $E(B - V) = 0.10$  would imply  $\log[N(\text{H})] \sim 20.7 \pm 0.3$  toward both stars.

(4) The upper limit on  $N(\text{O I})$  (from the non-detection of the weak  $\lambda 1355$  line) toward HD 72127A may be used to place a corresponding upper limit on  $N(\text{H I})$ , as the two species are strongly coupled via charge exchange. The observed  $\log[N(\text{O I})] < 17.14$  implies  $\log[N(\text{H I})] < 20.55$ , for a solar oxygen abundance of  $-3.31$  dex and a typical ‘warm cloud’ depletion of  $-0.1$  dex (e.g., Cartledge et al. 2004).

(5) The equivalent widths observed for the weak lines of typically moderately depleted Mg II (1239 and 1240 Å) and for the strong lines of typically undepleted S II (1250, 1253, and 1259 Å) are very similar toward the two stars (Table 1; Wallerstein et al. 1995b) – suggesting that  $N(\text{H})$  also is similar toward both.

(6) The upper limit on  $\log[N(\text{CH})] < 12.4$  obtained from the UVES spectra suggests that  $\log[N(\text{H}_2)]$  is less than 20.0 toward both stars (e.g., Welty et al. 2006).

As the different indicators (photometry, optical spectra, UV spectra) are from different epochs, these comparisons and estimates are somewhat uncertain, given the observed temporal variations for some interstellar quantities in both sight lines. None the less, in view of the various estimates and limits, we have adopted  $\log[N(\text{H I})] \sim \log[N(\text{H})] \sim 20.4$ ,

**Table 5.** Abundance and depletion data (HD 72127A).

Element	Solar	D(Warm)/ D(Cold)	main	D(72127A) outlier	total
O	8.69	-0.1/-0.2	<0.03	-	< -0.05
Na	6.30	-0.6/-0.6	-	-	-
Mg	7.55	-0.6/-1.3	-	-	-0.66
Si	7.54	-0.4/-1.3	-0.63	-0.15	-0.51
Ca	6.34	-2.0/-3.6	-2.38	-	-1.75
Ti	4.92	-1.3/-2.9	-1.77	-1.25	-1.64
Cr	5.65	-1.2/-2.2	-1.41	-0.82	-1.25
Fe	7.47	-1.3/-2.2	-1.49	-0.61	-1.18
Ni	6.22	-1.4/-2.3	-1.52	-0.53	-1.14
Zn	4.63	-0.2/-0.4	-0.26	-	-0.31
Ge	3.62	-0.6/-0.9	-0.69	-	-

Solar abundances are from Lodders (2003). Representative warm and cold cloud depletions are updates of values in Welty et al. (1999b). Last three columns give depletions for HD 72127A: main components (10–20 km s<sup>-1</sup>), all other components, and all components, respectively. Those depletions assume  $\log[N(\text{H})] = 20.32, 19.60,$  and  $20.40$  dex for the three groups.

with an uncertainty of perhaps  $\pm 50$  percent, toward both HD 72127A and HD 72127B.

The fits to the Zn II, S II, and Si II profiles toward HD 72127A suggest that roughly 80–90 percent of the total H I is found in the components between 10 and 20 km s<sup>-1</sup> (‘main components’), with the remainder in the outlying higher velocity components. On the other hand, roughly 60 percent of the Fe II and Ni II is found in the outlying components. Inspection of the ratios of the column densities of typically depleted species to that of (nearly) undepleted Zn II (e.g., Fe II/Zn II; last column of Table 3) indicates that the depletions in the outlying components are significantly less severe than those in the main components. If the adopted total  $N(\text{H})$  is apportioned to the main components ( $2.1 \times 10^{20}$  cm<sup>-2</sup>) and the outlying components ( $4 \times 10^{19}$  cm<sup>-2</sup>), then the depletions may be estimated separately for those two component groups (Table 5). For the main components, the resulting depletions are broadly consistent (within the uncertainties) with those in ‘warm diffuse’ clouds in the Galactic disc (Savage & Sembach 1996; Welty et al. 1999); for the outlying components, the depletions are more similar to those in Galactic halo clouds. The similarities in  $E(B - V)$ ,  $N(\text{Ti II})$ , and the equivalent widths of the 5780 Å DIB and the lines of Mg II and S II for both HD 72127A and HD 72127B (Wallerstein et al. 1995b; this paper) suggest that both the total  $N(\text{H})$  and the average depletions are also similar (within factors of about 2) for the two lines of sight; the depletions may be slightly less severe toward HD 72127B.

Examination of the profiles of the Al III lines at 1854 and 1862 Å may provide some insight into the distribution of ionized gas toward HD 72127A. Integrating the apparent optical depths over the profiles yields a total  $N(\text{Al III})$  of about  $1.7 \times 10^{13}$  cm<sup>-2</sup> in each case, so the lines do not appear to be significantly saturated. There is very little Al III absorption at the velocities of the main components between 10 and 20 km s<sup>-1</sup> – which thus are likely to be predominantly neutral. The Al III absorption at higher and lower velocities (especially the strong absorption centred at about

35 km s<sup>-1</sup>) signals the presence of some ionized gas at those outlying velocities. Crude fits to the Al II line at 1670 Å (using the Fe II component structure), however, suggest that the Al II/Al III ratio is about 3–4 (on average) for those outlying components – so that the fraction of ionized gas may be relatively small there as well. Uncertainties as to the amounts of H II and X III (i.e., the second ions of elements whose first ions X II are dominant in H I gas) present in the outlying components imply corresponding uncertainties in the depletions estimated for those components in Table 5.

### 3.2 Ca II/Na I ratios

The Ca II/Na I ratio is usually considered to be an indicator of the (highly variable) depletion of calcium, and can range from  $\lesssim 0.01$  in cold, dense clouds (where calcium generally is severely depleted) to  $\gtrsim 10$  in warm, diffuse gas (where some fraction of the calcium has been returned to the gas phase). Hobbs et al. (1982) found unusually high Ca II/Na I ratios ( $>9$ ) for all five of the components toward HD 72127A seen in 1977. The detailed fits reported by Hobbs et al. (1991), however, yielded average ratios ranging from 1.4 for the component at +13 km s<sup>-1</sup> (with strongest Na I) to  $>30$  for the components at -19 and -8 km s<sup>-1</sup>, for observations between 1981 and 1988. Fits to the 2003 UVES spectra imply Ca II/Na I ratios ranging from 0.6 (at +13 km s<sup>-1</sup>) to  $>20$  (at -15, +40, and +55 km s<sup>-1</sup>) toward HD 72127A and from 2.7 (at +11 km s<sup>-1</sup>) to  $>40$  (at -16 and +54 km s<sup>-1</sup>) toward HD 72127B. At least some of the differences between the current and former results are likely due to the more detailed and precise component information obtained from the more recent spectra and to the availability of  $\lambda 3302$  data for Na I. The depletions that would be inferred from the Ca II/Na I ratios in the different components thus are consistent with the depletion levels determined more directly from the various dominant species in the previous section.

### 3.3 Temporal variations

Temporal variations over the past 30 years in the complex profiles of Na I and Ca II toward HD 72127A have been well documented. Hobbs et al. (1982) noted the appearance of a ‘new’ component at +15 km s<sup>-1</sup> in a Ca II spectrum obtained in 1981 April. Detailed fits to that same spectrum (and others obtained through 1988 Dec) revealed both additional weaker components and variations in the column densities and/or velocities of most of the Ca II components between -15 and +17 km s<sup>-1</sup> (Hobbs et al. 1991). An ultra-high resolution Ca II spectrum obtained in 1994 Feb revealed continued variations over that velocity range, more complex structure between -20 and +40 km s<sup>-1</sup>, and new variations between +25 and +35 km s<sup>-1</sup> (Fig. 1; Welty et al. 1996; see also Cha & Sembach 2000). The UVES Ca II spectrum (2003 Nov) shown in Fig. 1 indicates further changes in the component column densities over most of the velocity range and continued evolution of the structure between +25 and +35 km s<sup>-1</sup>. The component velocities found for the UVES spectrum are very similar, however, to those determined from spectra of comparable resolution obtained in 1994 and 1996 (Cha & Sembach 2000), when allowance is made for differences in adopted component structure (Table 6). The most noticeable change in the Na I profile toward

**Table 6.** Ca II component velocities (1988–2003).

1988 Dec	1994 Feb	1994 Feb	1996 J/F	2003 Nov
HD 72127A				
				-27.7
-18.8	-17.7			
-14.6	-15.3	-15	-15	-15.4
	-9.1			
-8.0	-8.2	-8	-8	-8.2
	-0.8			
	2.0	3	3	2.9
3.5	4.6			
	7.8			
11.0	12.7			12.6
	13.2			
17.4	14.3	14	14	
	22.1			18.3
27.7	29.8	30	29	26.0
	31.1			32.3
	38.5			
39.8	40.9	41	40	40.0
54.8	53.9	55	55	54.7
59.8	58.2			
HD 72127B				
			-15	-16.0
			-6	-5.4
				4.3
			13	10.5
				21.0
			30	29.4
				35.7
			40	42.9
			55	53.8
				88.0
				96.9

Velocities are heliocentric; ultra-high resolution spectrum from 1994 Feb used as standard for HD 72127A. References: 1988 Dec (Hobbs et al. 1991); 1994 Feb (Welty et al. 1996); 1994 Feb and 1996 J/F (Cha & Sembach 2000); 2003 Nov (this paper). See Hobbs et al. (1982, 1991) for values from previous epochs.

HD 72127A since 1988 is the appearance of a distinct component near +4 km s<sup>-1</sup> (Cha & Sembach 2000; this paper) superimposed on (or in place of) the smooth, broad shoulder seen in previous (higher resolution) spectra short-ward of the strongest Na I absorption near +13 km s<sup>-1</sup>.

Unfortunately, much less information is available for the interstellar lines toward the fainter HD 72127B. Component velocities for Ca II reported by Hobbs et al. (1982) and by Cha & Sembach (2000) are reasonably consistent with those determined from the UVES spectrum (Table 6), and the 1996 line profile plotted by Cha & Sembach (2000) appears to be very similar to the 2003 UVES profile plotted in Fig. 1 (though the total equivalent width was smaller in 2003). The weak high-velocity components found in the UVES spectrum of HD 72127B (similar to those seen toward several other stars in the Vela region; e.g., Wallerstein et al. 1980; Danks & Sembach 1995) do not appear to be present in the 1996 spectrum, however. The lines from several of the trace neutral species measured in the 2003 UVES spectrum of HD 72127B are significantly stronger than pre-



viously reported: the equivalent width of the Na I  $\lambda 5895$  line (188 mÅ) is roughly twice the 95 mÅ value listed by Hobbs et al. (1982), while the equivalent width of the Ca I  $\lambda 4226$  line (16 mÅ) is more than three times the upper limit given by Wallerstein & Gilroy (1992).

### 3.4 Spatial variations

Thackeray (1974) first called attention to differences in the profiles of the strong, broad Ca II K lines toward HD 72127A and HD 72127B; Hobbs et al. (1982) subsequently noted differences in the velocity structures seen in both Ca II and Na I. Higher resolution Ca II spectra obtained by Cha & Sembach (2000) indicate that while the overall velocity extent of the absorption is very similar toward the two stars, the detailed column density distribution (as a function of velocity) is quite different. Wallerstein et al. (1995b) found similar equivalent widths for UV lines of Mg II and Si II (but differences in the strengths of lines from P II and Ge II) in *HST*/G160M spectra of the two stars. Possible differences in detailed component structure (as seen for Ca II) could not be discerned in those moderate-resolution UV spectra, however.

The UVES spectra of HD 72127A and HD 72127B shown in Figs. 1 and 2 provide both a more recent snapshot of the differences in Na I and Ca II and indications of similarities and differences for lines from several other species. Toward HD 72127B, the main component(s) near +11 to +13 km s<sup>-1</sup> are stronger in both Na I and Ca II than those toward HD 72127A, but the outlying components generally are weaker. The overall structure and relative column densities are more similar for Na I than for Ca II – opposite the general trend for observations of those two species toward other binary systems (Meyer 1990; Watson & Meyer 1996). The weak Na I  $\lambda 3302$  doublet lines are similar in strength toward the two stars, but there are modest differences in the profiles of the Ti II  $\lambda 3383$  line and very striking differences in the lines from previously undetected Ca I, Cr I, and Fe I (which are much stronger toward HD 72127B; see next section).

### 3.5 Trace neutral species toward HD 72127B

The absorption lines from several trace neutral species are unusually strong in the 2003 UVES spectrum of HD 72127B. For the  $N(\text{H}) \sim 2.5 \times 10^{20}$  cm<sup>-2</sup> estimated above, the column density of Na I is somewhat higher than usual (Welty & Hobbs 2001), and the column densities of Ca I, Cr I, and Fe I are remarkably high (Welty et al. 2003) – especially as most of the absorption from those trace neutral species is found in the (apparently) single strong component near +11 km s<sup>-1</sup>. The column density of Ca I, for example, is among the highest known for any Galactic sight line; comparable values generally are seen only for sight lines with much higher  $E(B - V)$  and/or  $N(\text{H})$ . Absorption from interstellar Cr I had previously been seen only toward  $\zeta$  Oph (Meyer & Roth 1990), with an equivalent width  $W(3578) = 0.25 \pm 0.06$  mÅ for the strongest line at 3578 Å in the main (B) components near -15 km s<sup>-1</sup>, which have  $N(\text{H}) \sim 14 \times 10^{20}$  cm<sup>-2</sup>. Toward HD 72127B, the Cr I  $\lambda 3578$  line has  $W(3578) = 5.4 \pm 0.7$  mÅ, and five other Cr I lines are

**Table 7.** Ratios of trace neutral species (predicted and observed).

Location	Mg I/Na I	Ca I/Na I	Cr I/Na I	Fe I/Na I
Solar (7000 K)	+1.55	+0.08	-2.43	+0.92
Solar (3000 K)	+0.52	-1.65	-2.43	+0.02
Solar (100 K)	+0.60	-1.29	-2.43	+0.10
Warm (7000 K)	+1.55	-1.32	-3.03	+0.22
Warm (3000 K)	+0.52	-3.05	-3.03	-0.68
Cold (100 K)	-0.10	-4.29	-4.03	-1.50
HD 72127A	+0.46	-2.88	< -1.85	-1.69
HD 72127B	-	-1.90	-1.46	-0.79
23 Ori SLV	+0.39	-3.21	< -2.82	-2.07
$\zeta$ Oph B	-0.05	-4.39	-4.05	-2.62
$\epsilon$ Ori (+3)	+0.81	-1.77	-	-
HD 90177 (-40)	-	-1.37	-	+0.36
HD 94910 (-54)	-	-1.14	-	+0.54
Sk-67 5 (+261)	-	> -0.85	-	> +1.05
Sk-68 52 (+307)	-	-1.51	-	< +0.31
SN1987A (+65)	-	-1.57	-	-
SN1987A (+165)	-	> -0.83	-	-
SN1987A (+216)	-	-1.74	-	-

Entries are  $\log [N(\text{X})/N(\text{Y})]$ ; limits are  $3\sigma$ . Predicted ratios for solar, warm cloud, and cold cloud abundances use the solar abundances and representative depletions from Table 5 and ionization equilibrium calculations as in eqn. 1 (see also Welty et al. 1999a). Predicted values for Ca I are for  $n_e = 1.0$  cm<sup>-3</sup>. Values for HD 90177 and HD 94910 are from Gnaniński & Krogulec (2008); values for Sk-67 5 and Sk-68 52 are from Welty & Crowther (in preparation); values for SN1987A are from Welty et al. (1999a).

seen at greater than  $3\sigma$  significance – all at the same velocity and with equivalent widths consistent with the relative  $f$ -values (Table 1).

Such (relatively) strong absorption from Ca I and/or Fe I has recently been noted in a few other sight lines. Table 7 compares the ratios of several trace neutral species X I/Na I – as observed toward HD 72127A, HD 72127B, and several other targets – with the values that would be predicted assuming ionization equilibrium under various conditions. The last six sight lines in the table exhibit components with even more extreme values of Ca I/Na I and/or Fe I/Na I; the well-studied sight lines toward 23 Ori (Welty et al. 1999b) and  $\zeta$  Oph (e.g., Welty & Hobbs 2001; Welty et al. 2003) are included for comparison. The clouds toward HD 90177 and HD 94910 are two of the so-called ‘CaFe’ clouds identified by Bondar et al. (2007) and discussed by Gnaniński & Krogulec (2008). Still higher values of Ca I/Na I and/or Fe I/Na I are seen in components toward three targets in the Large Magellanic Cloud (Welty et al. 1999a; Welty & Crowther, in preparation). In two of those LMC components, no absorption is detected in the Na I D lines, with upper limits on  $N(\text{Na I})$  of order  $1\text{--}4 \times 10^{10}$  cm<sup>-2</sup>.

Observations of quasar absorption-line systems have begun to yield detections of weak lines from various trace neutral species (besides the commonly observed Mg I) in higher redshift systems. For example, Si I, Fe I, and several other neutral species have been detected (along with a modest amount of H<sub>2</sub>) in a sub-Damped Lyman  $\alpha$  system at  $z \sim 1.15$  (Quast, Reimers, & Baade 2008). Unexpectedly strong

absorption from Si I, Ca I, and Fe I has also been observed in a weak Mg II absorber at  $z \sim 0.45$  (D’Odorico 2007)<sup>2</sup>. Absorption from Na I has not yet been observed in those systems, however.

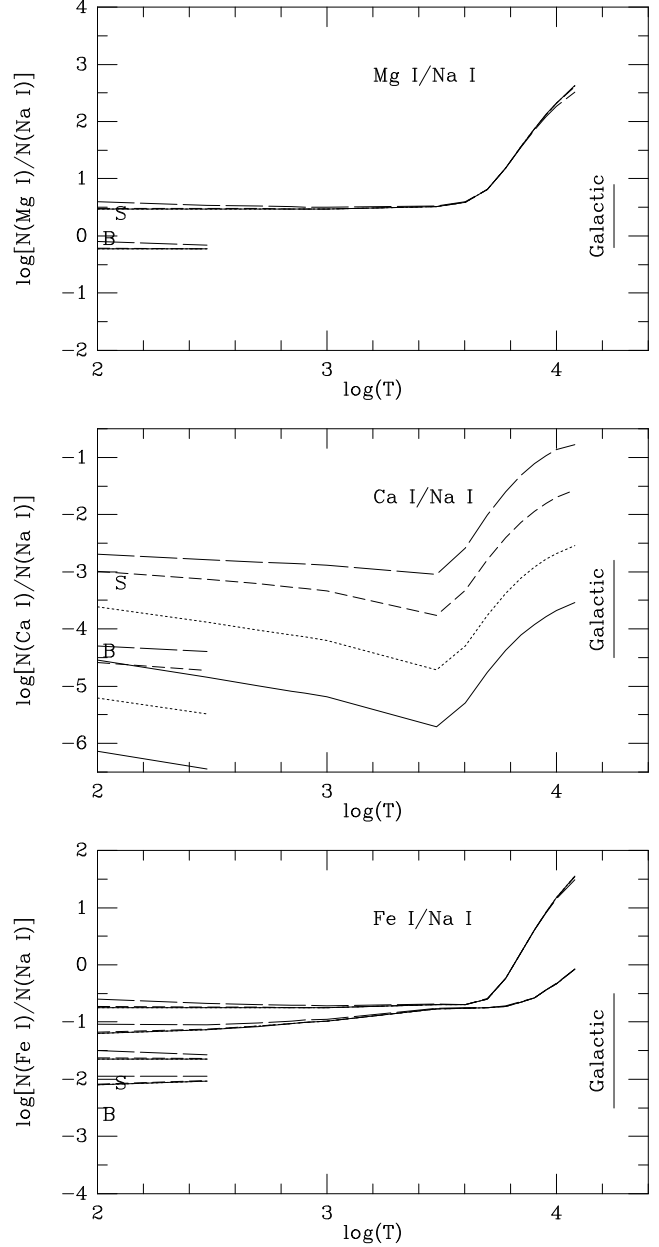
Consideration of the physical conditions and ionization equilibrium in the main cloud toward HD 72127B might provide some insight into the high observed abundances of the trace neutral species in those various contexts. Wallerstein et al. (1995b) found a relatively high fraction of the Ca I toward HD 72127B to be in the excited fine-structure states – indicative of a relatively high thermal pressure ( $n_{\text{H}}T$ ) in the gas. High densities would be expected to favor the trace neutral species; Ca I (and several other neutral species) can be enhanced via dielectronic recombination in warmer gas. While the width of the Ca I component at +13 km s<sup>-1</sup> toward HD 72127A ( $b = 0.6$  km s<sup>-1</sup>; Welty et al. 2003) places an upper limit on the temperature of  $T \lesssim 850$  K for that component (so that dielectronic recombination would not be significant there), the main Ca I component toward HD 72127B may be somewhat broader. Higher resolution spectra of HD 72127B would be needed to place a firmer limit on the temperature (and the role of dielectronic recombination) in the main component in that sight line. The Ca I/Ca II ratio (0.0055) in the main component toward HD 72127B, however, is very similar to the ratios seen in other Galactic sight lines (e.g., Welty et al. 2003) and is only a factor of two higher than the ratio (0.0026) found in the main component toward HD 72127A – which would seem to suggest that Ca I is not greatly enhanced relative to Ca II and that the electron density  $n_e$  is not especially high.

Fig. 4 shows the ratios  $X\text{I}/\text{Na I}$  (for  $X = \text{Mg}, \text{Ca},$  and  $\text{Fe}$ ) that would be predicted for equilibrium between ionization (radiative plus collisional) and recombination (radiative plus dielectronic), as functions of temperature (as in Fig. 11 of Welty et al. 1999a, for example). Those earlier calculations (which assumed ‘warm cloud’ depletions) have been adjusted here for total gas phase elemental abundances characterized also by the patterns seen in the solar system (Lodders 2003) and in interstellar clouds exhibiting ‘cold cloud’ depletions (e.g., Savage & Sembach 1996; Welty et al. 1999b; see Table 5). The first six lines of Table 7 list the predicted ratios for several representative combinations of depletion and temperature. For Mg, Cr, and Fe – for which the first ions  $X\text{II}$  should be dominant – the predicted ratios are given by

$$\frac{X\text{I}}{\text{Na I}} = \frac{A_X \delta_X \alpha_X}{A_{\text{Na}} \delta_{\text{Na}} \alpha_{\text{Na}}} \frac{(\alpha_{\text{Na}} n_e + \Gamma_{\text{Na}} + c_{\text{Na}} n_e)}{(\alpha_X n_e + \Gamma_X + c_X n_e)}, \quad (1)$$

where  $A_X$  and  $\delta_X$  are the solar abundance and depletion of element  $X$ , respectively. The calculation for calcium is slightly more complicated, as Ca III must also be considered. The adopted photoionization rates ( $\Gamma_X$ ) are taken in most cases from Péquignot & Aldrovandi (1986), assuming the WJ1 radiation field (de Boer et al. 1973); the collisional

<sup>2</sup> Based on comparisons with Galactic sight lines, D’Odorico (2007) infers  $\log[N(\text{H})] \sim 20.5\text{--}21.5$  – and thus a very low metallicity – for that absorber. The Galactic sight lines, however, are typically characterized by significant depletions of the various refractory elements. The  $N(\text{H})$  in the weak Mg II system (where the depletions are likely much less severe) may well be much lower, and the metallicity correspondingly higher.



**Figure 4.** Predicted ratios  $X\text{I}/\text{Na I}$  – for  $X = \text{Mg}, \text{Ca},$  and  $\text{Fe}$  – as functions of temperature. The calculations assume equilibrium between ionization (radiative and collisional) and recombination (radiative and dielectronic), warm cloud depletions, and  $n_e = 0.001, 0.01, 0.1,$  or  $1.0$  cm<sup>-3</sup> (lower to upper curves in each panel). The lower partial curves (from 100 to 300 K) show the ratios for cold cloud depletions. The increases at higher temperatures are due to dielectronic recombination to Mg I, Ca I, and Fe I. The lower set of curves for Fe I shows the predictions for the photoionization and recombination rates calculated by Nahar et al. (1997). The letters ‘S’ and ‘B’ mark the ratios observed for the 23 Ori SLV components and the  $\zeta$  Oph B components, respectively; the bar at right shows the range for each ratio observed in the local Galactic ISM.

ionization rates ( $c_X$ ) are taken from Shull & Van Steenberg (1982). The total (radiative plus dielectronic) recombination rate coefficients ( $\alpha_X$ ) are calculated from the parameters given by Aldrovandi & Péquignot (1973, 1974), Shull & Van Steenberg (1982), and/or Péquignot & Aldrovandi (1986). The lower set of curves for Fe I shows the ratios predicted using the photoionization and (total) recombination rates computed by Nahar, Bautista, & Pradhan (1997). For Cr I,  $\Gamma_{Cr} = 8 \times 10^{-10} \text{ s}^{-1}$  was estimated by Meyer & Roth (1990), and  $\alpha_{Cr}$  has been set to  $6 \times 10^{-12} \text{ cm}^3 \text{ s}^{-1}$  (for  $T = 100 \text{ K}$ ), similar to the values determined for radiative recombination to a number of other trace neutral species (Péquignot & Aldrovandi 1986); the temperature dependence of  $\alpha_{Cr}$  is assumed to be the same as for  $\alpha_{Na}$  (i.e., with no significant contribution from dielectronic recombination for  $T < 12000 \text{ K}$ ; see comments below, however). If the recombination is dominated instead by charge exchange with large molecules or small grains (Lepp et al. 1988; Weingartner & Draine 2001; Liszt 2003; Welty et al. 2003), and if the resulting neutrals do not stick to the grains (sticking parameter  $s = 0$ ), then the predicted ratios change by at most 0.1 dex.

The predicted ratios for Mg I, Ca I, and Fe I shown in Fig. 4 exhibit some common trends. At temperatures below about 3000 K, the ratios reflect primarily photoionization and radiative recombination – and are not very sensitive to the overall strength of the radiation field, the electron density  $n_e$ , or the temperature. Because Ca II is often a trace species, however, the Ca I/Na I ratio does depend on  $n_e$ . At somewhat higher temperatures, all the ratios increase due to dielectronic recombination (which does not significantly affect Na I until much higher temperatures) – starting at about 4000 K, 3000 K, and 5000 K for Mg I, Ca I, and Fe I, respectively (Aldrovandi & Péquignot 1973, 1974; Shull & Van Steenberg 1982).

For the main cloud(s) toward  $\zeta$  Oph, the observed ratios for Mg I, Ca I, and Cr I are in good agreement with the predicted cold cloud values (consistent with the depletions derived from the corresponding dominant species and the temperature inferred from H<sub>2</sub> rotational excitation). The ratio for Fe I is lower than the predicted cold cloud value by more than a factor of 10, however [but is not as deficient relative to the value predicted using the Nahar et al. (1997) rates]. Meyer & Roth (1990) remarked that the electron density estimated toward  $\zeta$  Oph from the Cr I/Cr II ratio was similar to the values obtained from other neutral/first ion ratios; Welty et al. (2003) noted that it is not uncommon for Fe I to be somewhat weaker than expected, relative to other trace neutral species. For the ‘strong low-velocity’ clouds toward 23 Ori (where some trace neutral species are relatively strong and the depletions are intermediate between the representative warm and cold cloud values; Welty et al. 1999b) and for the main cloud(s) toward HD 72127A (with warm cloud depletions), the observed ratios for Mg I and Ca I are closer to the predicted warm cloud values for  $T \sim 3000 \text{ K}$  (although the gas is likely much cooler than that in both cases), but the ratios for Fe I again are low by factors of 10–25. For the main cloud(s) toward HD 72127B, the observed ratios for both Ca I and Fe I are about a factor of 10 higher than those toward HD 72127A. The ratio for Ca I thus is closer to the value predicted for solar relative abundances than to that predicted for warm cloud abundances (for  $T \sim 3000 \text{ K}$ ), while the ratio for Fe I is consistent with the

predicted warm cloud value at that  $T$  (i.e., low compared to Ca I); the observed ratio for Cr I, however, is a factor of 10 higher than the predicted solar value.

As calcium, chromium, and iron usually are much more severely depleted into dust than is sodium, an enhancement of the neutral species Ca I, Cr I, and Fe I, relative to Na I, could be due to much less severe depletions. As noted above, dielectronic recombination can increase the abundances of Mg I, Ca I, and Fe I when the temperature exceeds about 4000 K, 3000 K, and 5000 K, respectively. The cloud at +65 km s<sup>-1</sup> toward SN1987A is relatively cold [as the Na I D lines at that velocity exhibit resolved hyperfine structure, with  $b \sim 0.3 \text{ km s}^{-1}$  (Pettini & Gillingham 1988; Welty & Crowther, in preparation)], but the ratios of various dominant species suggest that there is essentially no depletion there (Welty et al. 1999a). The observed Ca I/Na I ratio is within a factor of 2 of the predicted value for solar relative abundances at 100 K (i.e., a cold, dust-free cloud), though it is also consistent with the values predicted for somewhat warmer gas. For the component at +3 km s<sup>-1</sup> toward  $\epsilon$  Ori, the  $b$ -values for Na I, Ca I, and Ca II – all 0.36–0.38 km s<sup>-1</sup> – indicate that that cloud also is fairly cold (Welty et al. 1994, 1996, 2003). The slightly elevated Mg I/Na I ratio thus may reflect less severe depletion of magnesium there (and not dielectronic recombination). The still higher values of Ca I/Na I and/or Fe I/Na I seen in several other cases, however, would seem to imply some combination of mild (or negligible) depletions and dielectronic recombination in warmer gas (e.g., Gnacinski & Krogulec 2008)<sup>3</sup> – though the Ca I/Ca II ratios generally are not unusually high.

The strong observed absorption from Ca I, Cr I, and Fe I toward HD 72127B – relative to Na I and to the much weaker absorption from those species toward HD 72127A – also may suggest some combination of mild depletions and higher temperature. The similarities in the strengths of the 5780 Å DIB, the  $E(B - V)$  colour excesses, and the equivalent widths of the weak Mg II  $\lambda$ 1239,1240 lines toward HD 72127A and HD 72127B suggest that the total hydrogen column densities are similar for the two sight lines. The relatively small differences in the column densities of Na I and Ti II in the two sight lines (both overall and in the main components near +12 km s<sup>-1</sup>) and in the Ca I/Ca II ratios (in the main components) then suggest that differences in ionization and depletions could account for only part of the enhancement of Ca I, Cr I, and Fe I. The higher values for Ca I/Na I and Fe I/Na I toward HD 72127B could be explained, however, if the Ca I and Fe I were enhanced via dielectronic recombination, in gas with warm cloud depletions and  $T \gtrsim$

<sup>3</sup> Gnacinski & Krogulec (2008) assume that there is no depletion in the CaFe clouds – taking non-detections of CH to imply a lack of both H<sub>2</sub> and dust. We note, however, that there are many sight lines where CH is not detected (to similar limits), but which none the less have  $E(B - V)$  greater than zero, detections of H<sub>2</sub> (at column densities below the regime of self-shielding), and evidence from dominant species for at least moderate depletions. The high temperatures ( $\gtrsim 8000 \text{ K}$ ) derived for the CaFe clouds presumably reflect the ability of dielectronic recombination to produce the observed abundances of Ca I and Fe I in such warm gas. Allowance for depletions and for colder temperatures, however, could reduce the substantial discrepancies between their models and the Na I and K I observed for the ‘non-CaFe’ clouds.

5000 K. We conjecture that dielectronic recombination to Cr I might then account for the high Cr I/Na I ratio toward HD 72127B – and we would predict some enhancement of Mg I (which is not unusually strong toward HD 72127A), but no enhancement of Si I (for which dielectronic recombination becomes important at somewhat higher temperatures)<sup>4</sup>. If dielectronic recombination is responsible for the strong absorption from those trace neutral species toward HD 72127B, then there would be a significant difference in temperature for the main components toward HD 72127A and HD 72127B – over a distance of less than 2200 AU. We note, however, that the Ca I/Ca II ratio often seems to imply a higher  $n_e$  than other such trace/dominant ratios – even when the Ca I  $b$ -values place strong constraints on  $T$  (Welty et al. 2003) – so that high Ca I abundances are not necessarily due to dielectronic recombination in warm gas.

### 3.6 Location of gas

The location of the main absorption components at  $v \sim +10$  to  $+13$  km s<sup>-1</sup> ( $v_{\text{LSR}} \sim -3$  to  $0$  km s<sup>-1</sup>) toward HD 72127AB – with depletions apparently similar to those found in typical warm, diffuse disc clouds – is not known. The outlying components, with higher LSR velocities and much milder depletions, are very likely associated with the Vela SNR, at a distance of about  $250 \pm 30$  pc (Cha et al. 1999). Some absorption at low LSR velocities, however, is seen for stars closer than 200 pc – and appears to be located at distances less than about 130 pc (Cha et al. 2000). The foreground absorption is ‘patchy and inhomogeneous’ (Cha et al. 2000), and the highest column density of Na I seen toward any star foreground to the SNR is about  $7.2 \times 10^{11}$  cm<sup>-2</sup> (the  $v = 12.3$  km s<sup>-1</sup> component toward HD 72232, at less than 115 pc) – a factor of 3–5 lower than the values obtained for the main components toward HD 72127AB. The relatively weak Ca II absorption toward HD 72232 (15 mÅ; Cha & Sembach 2000) implies a Ca II column density of about  $2 \times 10^{11}$  cm<sup>-2</sup>; the corresponding Ca II/Na I ratio, about 0.3, is similar to the value found for the main component toward HD 72127A (Table 2). The much higher column densities and the continuing variations in both column density and velocity suggest that the bulk of the material in the main components toward HD 72127AB is associated with the SNR, but there is very likely some contribution from foreground material (at the same velocity) as well.

## 4 SUMMARY / CONCLUSIONS

New, moderately high resolution (FWHM = 4.5–4.9 km s<sup>-1</sup>) optical spectra of Na I and Ca II absorption toward HD 72127AB have provided additional evidence for both spatial and temporal variations in the complex interstellar absorption along the two sight lines. If the spatial differences are associated with material in the Vela SNR, they occur on

<sup>4</sup> After the initial submission of this paper, we received preliminary, partial calculations of the total recombination rate coefficients to Cr I (S. Nahar, private communication), which both confirm our assumptions regarding the recombination at  $T \lesssim 1000$  K and suggest that dielectronic recombination may indeed be significant below  $10^4$  K for Cr I.

scales of about 1100 AU. Fits to the absorption-line profiles seen in high-resolution (FWHM  $\sim 3.5$  km s<sup>-1</sup>) UV spectra of HD 72127A obtained with the *HST* GHRS have yielded abundances for a number of species (e.g., Si II, Fe II, Ni II, and Zn II) in the various velocity components discernible in the spectra. The main components at low LSR velocities have depletions similar to those found in warm, diffuse disc clouds; the generally weaker components at higher velocities have much milder depletions, more similar to those found in halo clouds. Similarities in  $E(B - V)$  and in the equivalent widths of the 5780 Å diffuse interstellar band and the UV lines of Mg II and Si II suggest that the total hydrogen column densities in the two sight lines are similar, with  $\log[N(\text{H}) (\text{cm}^{-2})] \sim 20.40$ . Similarities in the column densities of Ti II and Na I suggest that the depletions and ionization in the main components also are comparable (within factors of about 2). Several other trace neutral species – Ca I, Cr I, and Fe I – are much stronger toward HD 72127B, however. In particular, the column density of Cr I is about 30 times the value found for the main components toward  $\zeta$  Oph (the only other sight line in which Cr I has been detected) – even though  $N(\text{H})$  is a factor of about 6 lower toward HD 72127B. While an earlier high-resolution spectrum of Ca I toward HD 72127A indicates that the main component in that sight line has  $T \lesssim 900$  K, the strong absorption from Ca I and Fe I toward HD 72127B suggests that the main component there is much warmer –  $T \gtrsim 5000$  K – with dielectronic recombination largely responsible for the enhanced abundances of those neutral species. We conjecture that dielectronic recombination may also be responsible for the enhanced Cr I absorption toward HD 72127B, and predict that strong absorption will be found for Mg I as well.

It would be very useful to obtain high-resolution UV spectra of HD 72127B: Si II, Cr II, Fe II, and Zn II [to determine  $N(\text{H})$  and depletions and to compare with HD 72127A]; Mg I and Si I (to obtain constraints on the effect of dielectronic recombination); and C I (also toward HD 72127A; to estimate thermal pressures and densities in the various components). Higher resolution optical spectra of the trace neutral species would provide more stringent constraints on the temperature in the main component. Determination of the recombination behaviour of Cr II, as a function of temperature, would aid in understanding the high abundance of Cr I and the role of dielectronic recombination. Continued monitoring of the interstellar absorption toward these two stars could provide insights into the structure and properties of interface regions between warm and cool gas.

## ACKNOWLEDGMENTS

We are grateful to M. Rejkuba and M.-R. Cioni (ESO/Paranal) for their assistance with the UVES observations, to J. Thorburn for performing initial processing of the UVES data, and to S. Nahar for communicating preliminary results on the recombination to Cr I. T. S. acknowledges support from REU grant NSF-0353854 to the University of Chicago. This work has been supported by NASA Long-Term Space Astrophysics grants NAGW-4445 and NAG5-11413 to the University of Chicago. The GHRS data for

HD 72127A were originally obtained under NASA grant GO-2251.01-87A to the University of Chicago.

## REFERENCES

- Albert C. E. 1983, *ApJ*, 272, 509  
 Albert C. E. et al. 1993, *ApJS*, 88, 81  
 Aldrovandi S. M. V., Péquignot D. 1973, *A&A*, 25, 137  
 Aldrovandi S. M. V., Péquignot D. 1974, *Rev. Brasileira de Fisica*, 4, 491  
 Bondar A., Kozak M., Gnaciński P., Galazutdinov G. A., Beletsky Y., Krelowski J. 2007, *MNRAS*, 378, 893  
 Brogan C. L., Zauderer B. A., Lazio T. J., Goss W. M., DePree C. G., Faison M. D. 2005, *AJ*, 130, 698  
 Cartledge S. I. B., Lauroesch J. T., Meyer D. M., Sofia U. J. 2004, *ApJ*, 613, 1037  
 Cha A. N., Sembach K. R. 2000, *ApJ*, 126, 399  
 Cha A. N., Sembach K. R., Danks A. C. 1999, *ApJ*, 515, L25  
 Cha A. N., Sahu M. S., Moos H. W., Blaauw A. 2000, *ApJS*, 129, 281  
 Danks A. C., Sembach K. R. 1995, *AJ*, 109, 2627  
 de Boer K. S., Koppelaar K., Pottasch S. R. 1973, *A&A*, 28, 145  
 Deshpande A. A. 2000, *MNRAS*, 317, 199  
 Dieter N. H., Welch W. J., Romney J. D. 1976, *ApJ*, 206, L113  
 D'Odorico V. 2007, *A&A*, 470, 523  
 Frail D. A., Weisberg J. M., Cordes J. M., Mathers C. 1994, *ApJ*, 436, 144  
 Gnaciński P., Krogulec M. 2008, *A&A*, 477, 543  
 Gredel R., van Dishoeck E. F., Black J. H. 1991, *A&A*, 251, 625  
 Gredel R., van Dishoeck E. F., Black J. H. 1993, *A&A*, 269, 477  
 Haverkorn M., Goss W. M., eds 2007, *ASP Conf. Ser. Vol. 365, SINS – Small Ionized and Neutral Structures in the Diffuse Interstellar Medium*. Astron. Soc. Pac., San Francisco, CA  
 Heiles C. 1997, *ApJ*, 481, 193  
 Herbig G. H. 1993, *ApJ*, 407, 142  
 Herbig G. H. 1995, *ARA&A*, 33, 19  
 Hobbs L. M. 1984, *ApJS*, 56, 315  
 Hobbs L. M., Wallerstein G., Hu E. M. 1982, *ApJ*, 252, L17  
 Hobbs L. M., Ferlet R., Welty D. E., Wallerstein G. 1991, *ApJ*, 378, 586  
 Hunter I., Smoker J. V., Keenan F. P., Ledoux C., Jehin E., Cabanac R., Melo C., Bagnulo S. 2006, *MNRAS*, 367, 1478  
 Jenkins E. B., Tripp T. M. 2001, *ApJS*, 137, 297  
 Jenkins E. B., Silk J., Wallerstein G., Leep E. M. 1981, *ApJ*, 248, 977  
 Kemp S. N., Bates B., Lyons M. A. 1993, *A&A*, 278, 542  
 Lauroesch J. T., Meyer D. M., Watson J. K., Blades J. C. 1998, *ApJ*, 507, L89  
 Lepp S., Dalgarno A., van Dishoeck E. F., Black J. H. 1988, *ApJ*, 329, 418  
 Liszt H. S. 2003, *A&A*, 398, 621  
 Lodders K. 2003, *ApJ*, 591, 1220  
 Meyer D. M. 1990, *ApJ*, 364, L5  
 Meyer D. M., Roth, K. C. 1990, *ApJ*, 349, 91  
 Morton D. C. 2003, *ApJS*, 149, 205  
 Nahar S. N., Bautista M. A., Pradhan A. K. 1997, *ApJ*, 479, 497  
 Palmer B. A., Engelman R. 1983, *Atlas of the Thorium Spectrum*. Los Alamos Natl. Lab., Los Alamos, NM  
 Péquignot D., Aldrovandi S. M. V. 1986, *A&A*, 161, 169  
 Pettini M., Gillingham P. 1988, *AAO Newsletter*, 43  
 Points S. D., Lauroesch J. T., Meyer D. M. 2004, *PASP*, 116, 801  
 Quast R., Reimers D., Baade R. 2008, *A&A*, 477, 443  
 Rollinde E., Boissé P., Federman S. R., Pan K. 2003, *A&A*, 401, 215  
 Savage B. D., Sembach K. R. 1996, *ARA&A*, 34, 279  
 Shull J. M., Van Steenberg M. 1982, *ApJS*, 48, 95  
 Stanimirović S., Weisberg J. M., Hedden A., Devine K. E., Green J. T. 2003, *ApJ*, 598, L23  
 Stokes G. 1978, *ApJS*, 36, 115  
 Thackeray A. D. 1974, *Observatory*, 94, 55  
 Wallerstein G., Gilroy K. K. 1992, *AJ*, 103, 1346  
 Wallerstein G., Silk J., Jenkins E. B. 1980, *ApJ*, 240, 834  
 Wallerstein G., Vanture A., Jenkins E. B. 1995b, *ApJ*, 455, 590  
 Wallerstein G., Vanture A., Jenkins E. B., Fuller G. M. 1995a, *ApJ*, 449, 688  
 Watson J. K., Meyer D. M. 1996, *ApJ*, 473, L127  
 Weingartner J. C., Draine B. T. 2001, *ApJ*, 548, 296  
 Welty D. E. 2007, *ApJ*, 668, 1012  
 Welty D. E., Hobbs L. M. 2001, *ApJS*, 133, 345  
 Welty D. E., Frisch P. C., Sonneborn G., York D. G. 1999a, *ApJ*, 512, 636  
 Welty D. E., Hobbs L. M., Kulkarni V. P. 1994, *ApJ*, 436, 152  
 Welty D. E., Morton D. C., Hobbs L. M. 1996, *ApJS*, 106, 533  
 Welty D. E., Hobbs L. M., Lauroesch J. T., Morton D. C., Spitzer L., York D. G. 1999b, *ApJS*, 124, 465  
 Welty D. E., Hobbs L. M., Morton D. C. 2003, *ApJS*, 147, 61  
 Welty D. E., Federman S. R., Gredel R., Thorburn J. A., Lambert D. L. 2006, *ApJS*, 165, 138